Proof-of-concept for monitoring ground displacements in Tompkins County, NY using Persistent Scatterer Interferometric Synthetic Aperture Radar from the TerraSAR-X and Sentinel-1 satellites

Yusuf E. Molan, Matthew E. Pritchard, and Rowena B. Lohman

Department of Earth & Atmospheric Sciences

Cornell University, Ithaca, NY 14850 USA

Published: April 27, 2022

Summary

Underground mining and the pumping of fluids, such as the proposed Cornell University Earth Source Heat Project (ESH), can result in observable displacement of the Earth's surface that we can use to better understand the effects of those subsurface activities. Such surface movements can be monitored by ground surveying, but the process is labor intensive, limited in spatial extent, and potentially expensive. Here we test whether the established satellite monitoring of surface movements called Interferometric Synthetic Aperture Radar (InSAR) can be used in Tompkins County, NY as part of the ESH project with the goal of achieving a precision of a few mm/year over the areas of interest. We used data from two types of satellites: the TerraSAR-X and TanDEM-X (TSX) satellites of the German Space Agency (X-band, 3.1 cm radar wavelength) and the Sentinel-1 (S1) satellites of the European Space Agency (C-band, 5.6 cm radar wavelength). We find that both data can be used to detect sub-centimeter/yr deformation rates using Persistent Scatterer Interferometry (PSInSAR). We assess the precision of the inferred rates through comparisons with limited ground survey data and between satellites. PSInSAR selects only reliable pixels, aka persistent scatterers (PS), to be analyzed at the full spatial resolution of the data. Generally, man-made objects, buildings, pipes, roads, etc., are persistent scatterers whereas vegetation cover, fields, bare soil are excluded from further analysis. An analysis with snow-/rain-free TSX data showed that while removing snow covered and rainy images increases the PS population up to two times, the points are concentrated at locations that already have denser PS points. Further, snow-/rain-free images estimate almost the same deformation behavior as the full-stack data set does. In an area of known ground subsidence above an underground mine in Lansing, NY, our analysis revealed that TSX provides more PS points compared to S1. Although both datasets show inter-annual deformation rates that agree with the in situ observations, S1 possessed a higher noise level. With this lower precision level, S1 can be a reliable monitoring tool in the ESH area if the expected deformation is larger than 4-5 mm/yr and if the deforming area extends to at least 300 meters around the drilling site. Otherwise, TSX data should be considered for ground surface monitoring in the area. Based on our comparison with ground control points, we can expect to measure deformation rates of 1-2 mm/yr with TSX PSInSAR.

1. Background

To reduce carbon emissions, Cornell University (located in Ithaca, NY, part of Tompkins County, Figure 1) is studying whether it is possible to heat its campus with energy derived by extracting >60°C subsurface water. Cornell's Earth Source Heat (ESH) project (Gustafson and others 2018) will extract warm water from up to 3 km depth and will supply 5.6 MWth to heat the campus. Subsurface fluid removal, injection, and leakage can cause ground surface subsidence/uplift (for example, Lubitz and others, 2013; Heimlich and others, 2015). Surface deformation can damage infrastructure, buildings, and roads, but can also be used to better understand the ongoing changes and fluid/heat transport in the subsurface. Surface deformation can be measured by ground-based leveling and surveying, by use of the Global Navigation Satellite System (GNSS, which includes the Global Positioning System as well as other satellites), and by use of satellite or airborne Interferometric Synthetic Aperture Radar (InSAR). Ground-based leveling and surveying are long established techniques, but require installation of surveying monuments and laborious occupation of each monument each time a measurement is needed (for example, McClusky, S., and Tregoning, (2013)). GNSS systems collect three-dimensional (3D) deformation information at points that are either surveyed or have an antenna permanently installed (for example, McClusky, S., and Tregoning, (2013)).

InSAR provides all weather, day/night observations over large regions (10's to 100's of km in extent) at regular repeats at time intervals of days to weeks (Del Soldato and others, 2021). InSAR has been widely used to estimate surface deformation associated with natural processes and human-induced activities such as landslides, earthquakes, volcanos, groundwater extraction, and mining (for example, Bürgmann and others, 2000). InSAR measures just one component of motion (towards or away from the satellite) (for example, Rosen and others, 2000). InSAR measurements (like all other ground deformation measurements) can be affected by atmospheric effects, snow, and vegetation, all of which are prevalent in Tompkins County, NY.

Over the past few decades, various spaceborne SAR systems operating at different wavelengths and resolutions have been successfully used to detect surface deformation including ERS-1/2, ENVISAT ASAR, Radarsat-1/2, JERS1, ALOS/PALSAR, ALOS-2/PALSAR-2, SAOCOM-1, Cosmo-skyMed, Sentinel-1, and TerraSAR-X (for example, Bürgmann and others 2000; Rosen and others, 2000, Semple and others, 2017). In New York (NY) State, Semple and others (2017) and Valentino (2016) exploited ALOS1/PALSAR data to measure deformation of as much as 80 mm/yr related to a salt mine in the western part of the state. However, small scale deformation mapping in Tompkins County has been hampered by the lack of data acquired by earlier satellites (for example, ALOS-2, RSAT-1/2, CSK, Envisat, ERS). To date, conventional InSAR in Tompkins County has not been able to effectively distinguish mm/yr-level phase change due to ground deformation from phase artifacts related to atmospheric delay (for example, Valentino, 2016), and can be negatively impacted by other sorts of noise that cause the decorrelation of the InSAR phase. The InSAR coherence is sensitive to the changes in surface backscattering and can be influenced by temporal variations of surface backscattering due to precipitation, and the changes in vegetation, soil moisture, and snow depth. These changes deteriorate the accuracy of the estimated phase and affect its reliability. This study exploits two recently available satellite radar missions:the Sentinel-1 (S1) a and b satellites (radar wavelength of 5.6 cm, referred to as C-band) from the European Space Agency, and the tasking requested (and paid for) by this project from the TerraSAR-X and TanDEM-X (TSX) satellites (radar wavelength of 3.1 cm, referred to as X-band) of the German Space Agency. While the S1 satellites collect data over Tompkins County as part of their background mission, we had to request and pay for the TSX satellites to collect data over the study area.

To overcome the limitations which are involved in conventional InSAR, we used persistent scatterer interferometry (PSInSAR), also known as permanent scatterer interferometry (for example, Ferretti, 2001; Hooper and others, 2004). PSInSAR differs from conventional InSAR in that, instead of spatially averaging the data and then processing all pixels, it focuses only on "high quality" pixels that tend to be less affected by vegetation change, snow cover, etc. We aim to assess the ability of PSInSAR to map deformation in Tompkins County and, in particular, near the ESH site (Figure 1). In addition, we use the Cayuga Salt Mine area as a test site, because of the presence of known, previously measured by ground-based surveying, surface deformation (for example, Spectra Environmental Group and others (2000) and Neves (2015)) to evaluate the performance of the InSAR techniques we used to map the deformation. Although the area under land has not been mined since the 1990s and active mining is only occurring under the lake, it is known that subsidence is ongoing and likely to last for 200 years or more (Van Sambeek, 2013). Lubitz and others (2013) and Heimlich and others (2015) presented two successful examples of using PSInSAR to detect ground surface deformation in Germany related to geothermal energy extraction in areas with climate conditions and vegetation cover similar to Tompkins

County, NY. Here we demonstrate a use of PSInSAR to map mm-scale deformation in Tompkins County using TSX and S1 data between 2018-2021.

2. Data and Methodology

InSAR provides the capability to detect surface deformation along the radar line of sight (LOS) between the satellite and the ground. An interferogram shows the phase change between two SAR images that are taken from the same area but at different times. The phase change of an interferogram is a measure of the satellite's changing distance to a point on the ground as well as other factors (like changes in the amount of water vapor in the atmosphere, see Bürgmann and others 2000 and Rosen and others, 2000). The LOS change in the distance, $\triangle r$, will cause a change in phase $\triangle\varphi$ as

$$\triangle\varphi = \frac{4\pi}{\lambda}\triangle r + \varphi_n \quad (1)$$

where λ is the wavelength of the satellite and φ_n is the phase change due to other effects such as soil moisture, atmospheric artifacts, and noise (Bürgmann and others 2000 and Rosen and others, 2000).

The accuracy of InSAR-detected deformation is a function of the radar wavelength, spatial resolution, revisit time, and other parameters (for example, Rosen and others, 2000). We used SAR data from both the TSX and S1 satellites, which have different radar wavelengths, spatial resolutions and repeat times, to better understand the impact of these different characteristics on measurement quality. The TSX and S1 data cover an overlapping time period from Sep 17, 2018 to Aug 30, 2021 and Jan 2, 2020 to Aug 12, 2021, respectively. Figure 1 shows the outline of S1 and TSX tracks that were used in this study. Unlike TSX, which comes at a cost, S1 data is free and open-access. S1 has a minimum repeat visit time of 6 days over selected areas of the world (12 days in Tompkins County when every observation is acquired) and a ground pixel size of 3.0 m (range direction) by 14 m (azimuth direction). The TSX stripmap data used here has a repeat time of 11 days and a ground range resolution and azimuth resolution of about 2.5 m and 3.3 m, respectively. Not every possible image is acquired, due to satellite down time and competing observation requests, so there are time period gaps with more than 11 or 12 days between satellite observations in both the TSX and S1 datasets. The higher temporal and spatial resolution alone suggest that TSX may be a preferable choice for deformation mapping in the area. But, it has also been shown that longer radar wavelength observations can sometimes provide more precise measurements than shorter radar wavelengths, giving S1's wavelength of 5.6 cm a potential advantage. For example, Sandwell and others (2008), found that the phase noise of L-band ALOS PALSAR (24 cm radar wavelength) data is 1.6 times better than C-band ERS data (6 cm radar wavelength).

The S1 are freely available. The TSX data costs between $250-$3000 per scene for tasking and delivery, depending on whether it is purchased through an approved research project or a commercial project.

Therefore, our goal is to assess the relative precision of the two datasets to determine the achievable precision. This information and cost differences can be the basis of decisions about use of InSAR for future monitoring for an ESH system.

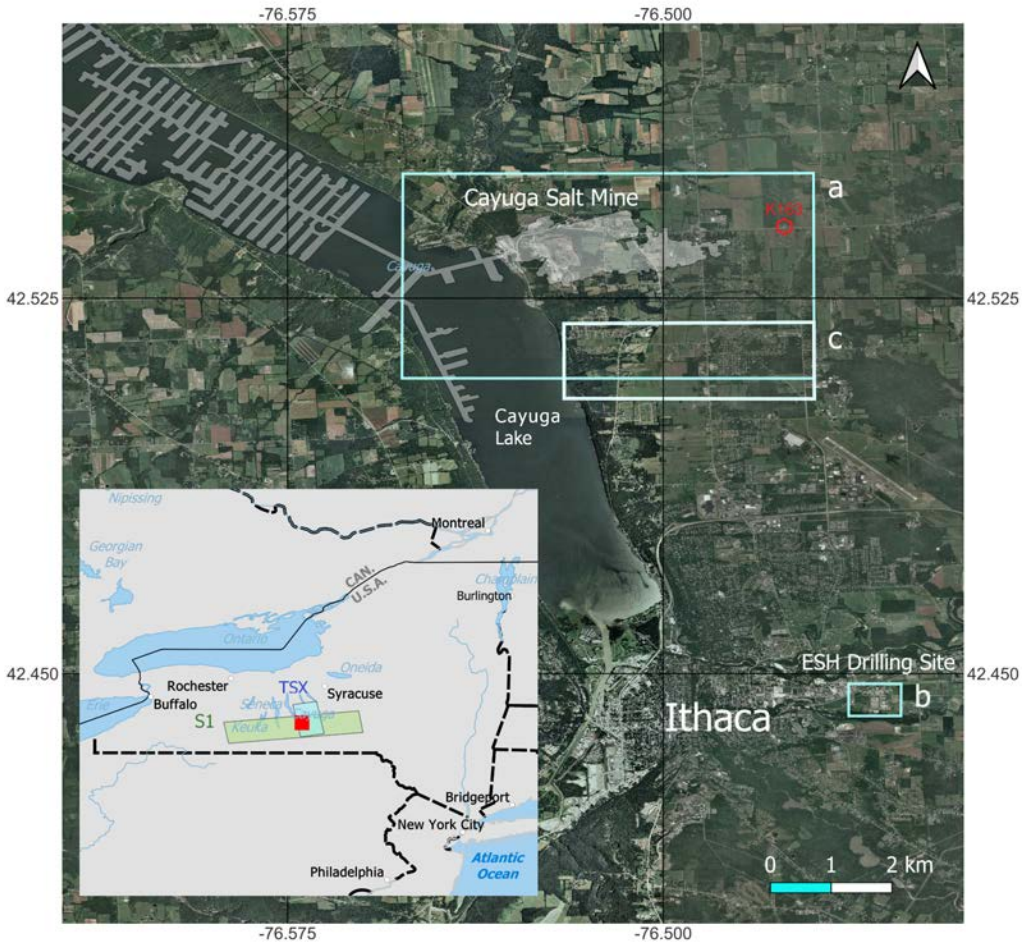

Figure 1. Overview map of the study area in Tompkins County, NY. Inset shows the study area with a red box on the New York State map. The S1 and TSX frames are shown in green and blue, respectively, on the inset map. The Cayuga Salt Mine region shown in Figure 4 and proposed ESH drilling area in Figure 12 are labeled "a", and "b", respectively. The reference area that is set to have zero deformation in the InSAR time series (see section 4.2) is labeled "c". The location of the ground-based surveying reference point (K163) is marked by a red hexagon.

Persistent scatterer interferometry (PSInSAR) (Ferretti 2001; Hooper and others, 2004) was exploited in this study. PSInSAR is a technique that uses the radar signal amplitude dispersion index to select pixels that tend to be the most stable across images acquired across multiple dates. One PSInSAR algorithm called StaMPS also uses the amplitude dispersion index to initially select persistent scatterers but exploits spatial phase stability analysis to select final persistent scatterers from the initially selected pixels (Hooper and others, 2007). We selected this technique as it removes noisy pixels that are the most sensitive to changing vegetation and snow. The remaining, more stable pixels have been shown in other regions to be reliable and to accurately estimate deformation at the mm/yr and even sub-mm/yr level (for example, Hooper and others, 2007, Ferretti and others, 2007, and Crosetto and others, 2015) when a series of images that is sufficiently well-sampled in time is available.

We analyzed an ascending S1 track (Path: 106, and Frame:133) with 49 images and an ascending TSX track (relative orbit number: 150) with 80 images using the StaMPS method (Hooper and others, 2004). The radar images are co-registered and prepared for PS analysis using the ISCE-2 software (Rosen and others, 2012). For each dataset, *i.e.,* 80 TSX images and 49 S1 images, the co-registration and preparing the image stack took 3-4 days of processing to be completed. The prepared, co-registered image stacks were then analyzed using StaMPS software (Hooper and others, 2004). PS analysis for each patch of the 30 patches of TSX and 20 patches of the S1 took 1-2 hours to be completed. The post-processing and map generation are done using python, Matlab, Jupyter, and QGIS software packages installed on Linux machines at the Remote Sensing Lab at Cornell University. We add the caveat that given the limited duration of this feasibility study (about 5 months), we did not have time to experiment with finding optimum parameters for processing the data and so future work might be able to obtain better results. In fact, we think the results are promising enough to merit further work.

We compare the PSInSAR results to vertical elevation differences at 38 benchmarks among six ground survey campaigns conducted between 1979-2021 (Neves (2015) and Mark Rowe, personal communication (2021)). In 1979, 1994, 2004, 2007, and 2014, these surveys were part of surface subsidence monitoring of the Cayuga Salt Mine as reported to the New York State Department of Environmental Conservation. In 2021, the survey was conducted by the Cayuga Lake Environmental Action Network (CLEAN). While surveyed latitude, longitude and elevations are provided from all six campaigns, we do not have details about the techniques used in the surveys nor their precision except for the 2021 survey. In 2021, Mark Rowe from Keystone Associates in Binghamton, NY, surveyed benchmarks using a 3" Leica TS16 total station with an estimated horizontal error of the traverse of about 1:30,000 and the vertical error was 1:80,000. All of the elevations for control points were adjusted to and based on benchmark K163 of the National Geodetic Survey (Figure 1). For surveys before 2021, we do not know the datum of the elevations, but as we argue below, we think that the National Geodetic Vertical Datum of 1929 (NGVD29) was used for all elevations.

3. Results

Figures 2 and 3 show maps of the extracted PS and the resulting average rates of displacement over the study area during the time periods covered by the TSX and S1 datasets, respectively. As expected, most of the PS points identified by StaMPS are found on stable, artificial structures like roads and buildings, and only a few points are found in forests or fields. While we generated displacement maps over the full extent of the radar imagery shown in Figure 1 inset, we only show a subset of the area in Figures 2 and 3, focusing on the ESH site and the known subsiding test site in the Lansing area. Note that supplementary materials including csv files of the entire regions shown in Figure 1 are available for download with this report, containing the longitude, latitude, and average displacement rate for all TSX PS points.

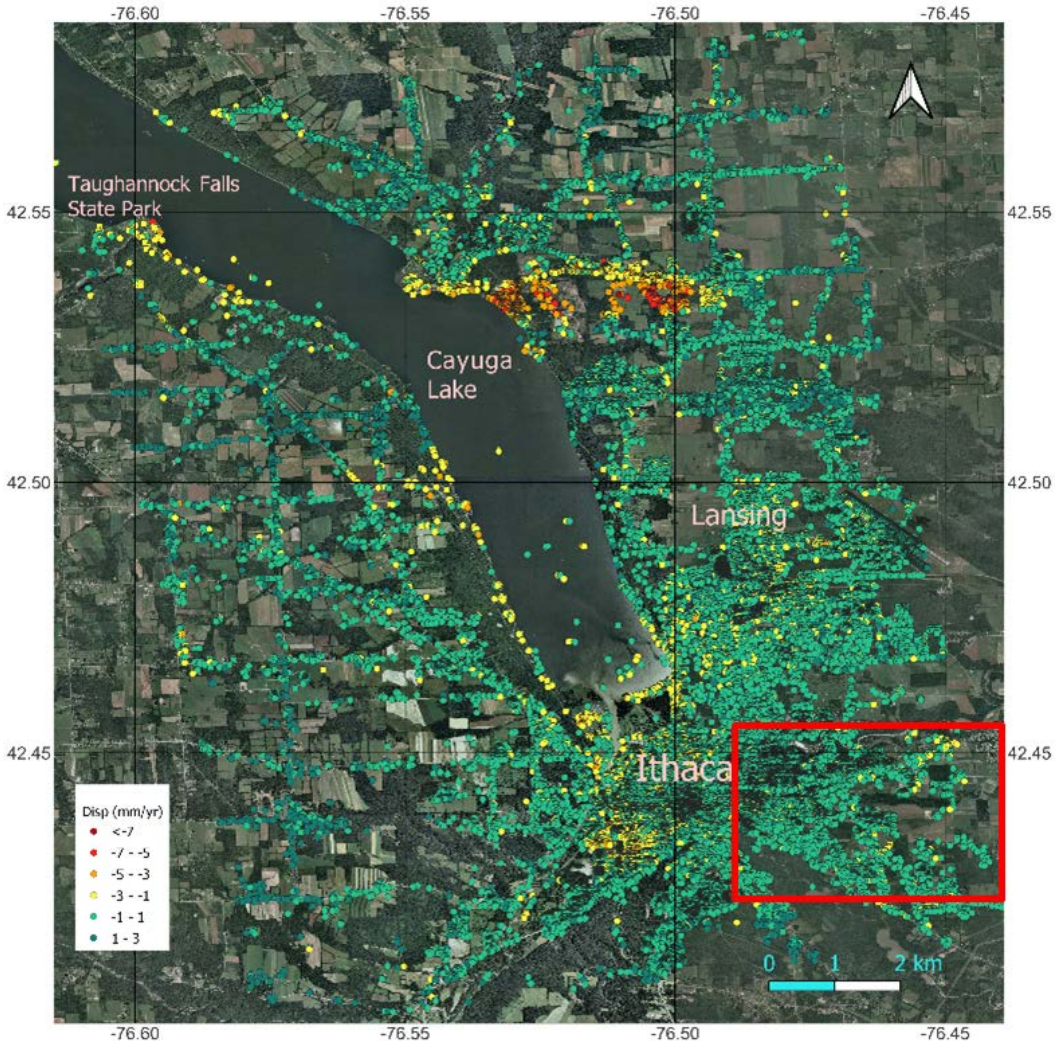

Figure 2. PSInSAR points using TSX data showing the rate of displacement in the radar line of sight averaged between 2018-2021 over the area of interest in this study (see reference map in Figure 1). The csv file of the map can be found in the supplementary data (TSX patches 4, 5, and 6 are plotted here). Data points in the water are artifacts and should be ignored. The red box is the area around the proposed ESH test site that is assumed to have no/negligible deformation and used to estimate the PSInSAR error bounds (section 4.2).

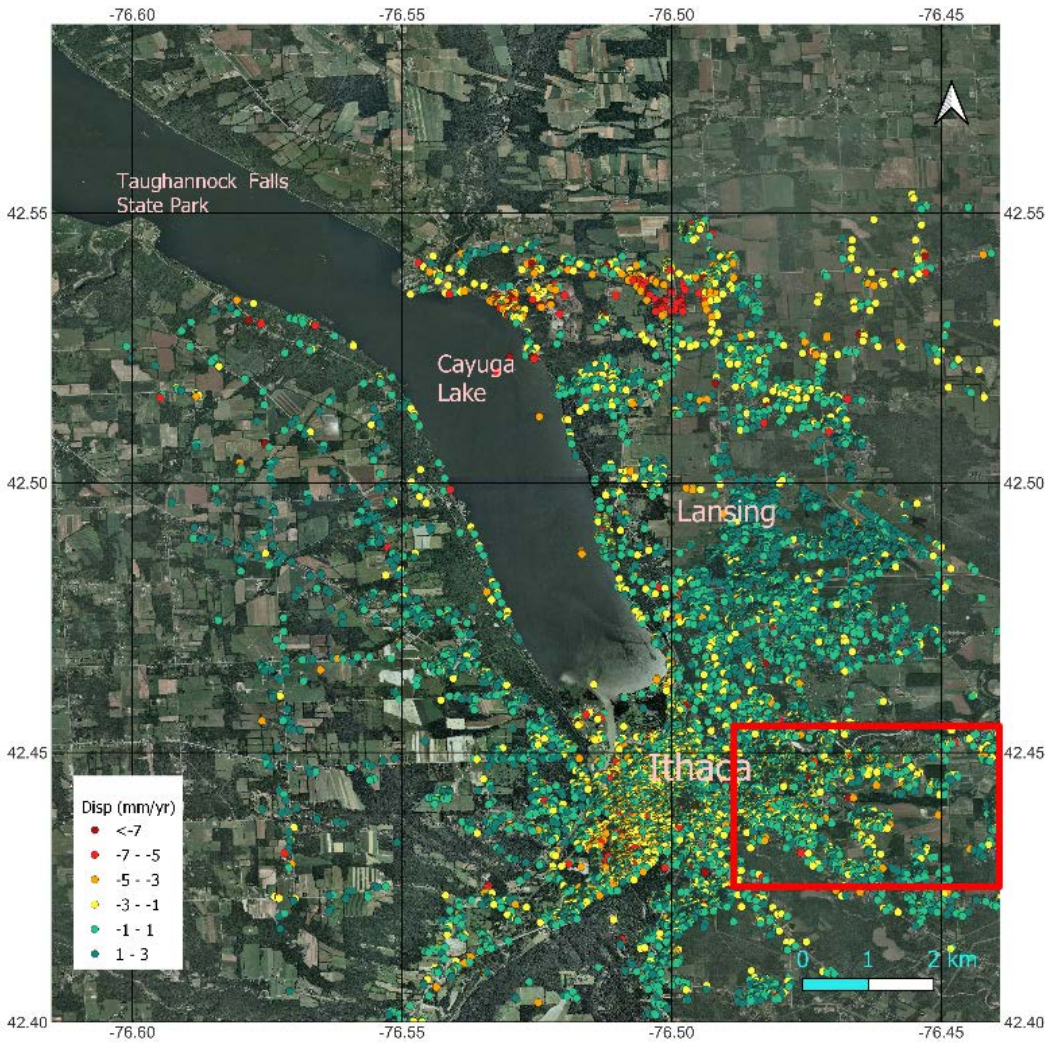

Figure 3. PSInSAR points using S1 data between 2020-2021 showing the rate of ground displacement in the radar line of sight over the area of interest in this study (see reference map in Figure 1). The csv files used to create this map can be found in the supplementary data (S1 patch 12 plotted here). Data points in the water are artifacts and should be ignored. See caption for Figure 2 for information about the red box.

The displacement rates are measured along the LOS between the satellite radar and the ground, such that both vertical and horizontal ground movements contribute to the measurement (see for example, Bürgmann and others, 2000). The incidence angle of the radar beam with respect to vertical is about 44 and 37 degrees, respectively for TSX and S1, so it is likely that most of the deformation being measured is vertical (although there is certainly a horizontal component as well). For Figure 4, we have converted the LOS to an inferred vertical displacement rate under the assumption that all ground deformation is vertical in order to facilitate comparison with ground surveying observations. The original displacement rates in the LOS are available in the supplemental material. The conversion is made using this equation:

inferred vertical displacement rate = LOS displacement rate/cosine (incidence angle)

Comparison of Figures 2 and 3 reveals that there are more PS points in the TSX dataset than the S1 dataset and that there is more scatter in the S1 dataset. This indicates a better precision and spatial coverage of TSX measurements that will be discussed further in Section 4. Both figures show that most rate measurements are near zero, with some negative values up to -10 mm/yr (indicating an increase in the radar line of sight, interpreted as subsidence) and fewer positive values (which would be consistent with ground uplift). Both the TSX and S1 datasets show a coherent region of inferred subsidence on the east side of Cayuga Lake with dimensions of about 3 km from East to West and 1 km North-South (shown in more detail in Figure 4). This area is near Lansing, NY, above an inactive portion of the subsurface salt mine that has been known to be subsiding for decades (see Section 4.2 for comparison of the PSInSAR and ground control points). Figure 4 again shows that the TSX data (panels a and b) have a higher density of stable PS points and less scatter among the inferred rate at these points than we see in the S1 data (panels C and D). Other areas of inferred subsidence are visible in Figure 2, such as the southwest shoreline of Cayuga Lake and at Taughannock Falls State Park, but we do not discuss these areas or others that are visible in the complete dataset in the supplemental material that could be the subjects for further work.

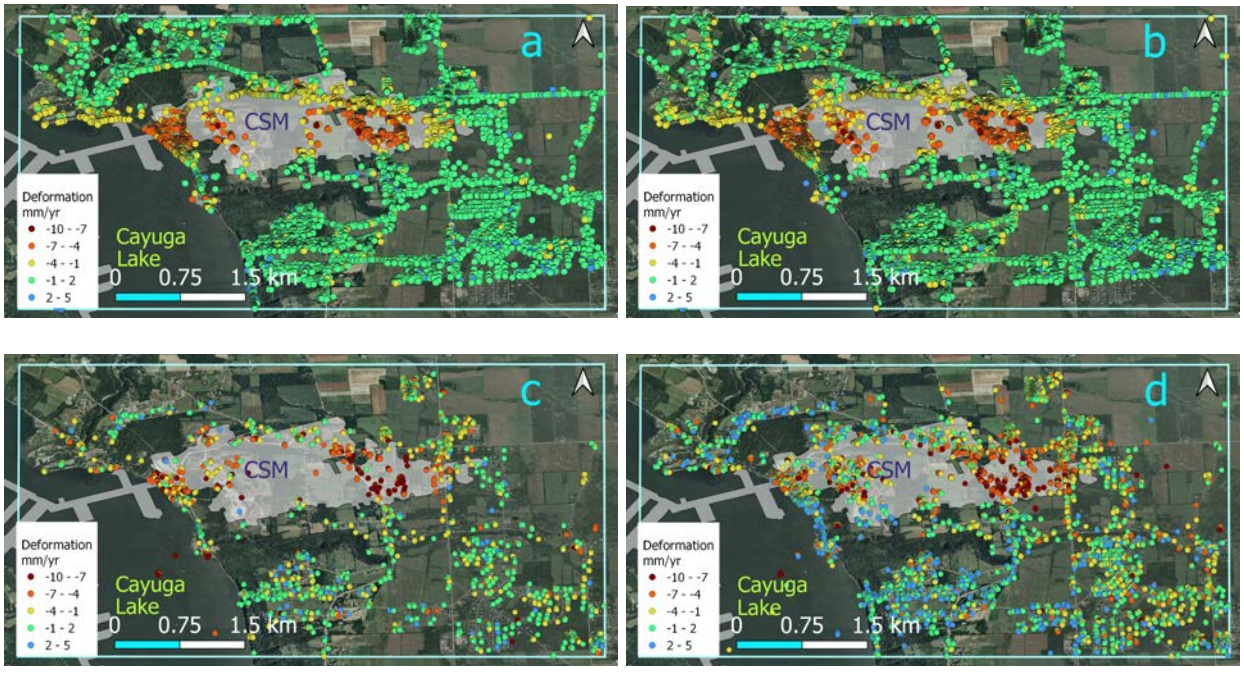

Figure 4. PSInSAR points and displacement rates extracted over Lansing and the Cayuga Salt Mine (CSM) using TSX (spanning 2018-2021)(a), TSX_srf (srf = snow and rain free, see section 4.1) (b), and S1 from 2020-2021 (c), and S1_srf (d) images. Displacements have been converted from the radar line sight to vertical deformation assuming that all deformation is vertical (see section 3 for details). The area shown in this figure is labeled "a" in Figure 1.

4. Discussion

In this section, we discuss the quality of PSInSAR measurements taken during the different months of the year and the precision of the measurements estimated by comparing the TSX and the S1 displacement rates to each other and to ground control points. We also assess the ability of the PSInSAR technique to detect ground deformation near the ESH site.

4.1. Feasibility of year-round InSAR measurements

We assessed the ability of the PSInSAR technique to make year-round measurements. InSAR deformation mapping requires that ground points remain stable and consistent between observations. In particular, there has been a concern that InSAR does not work during winter months because of wet snow cover (for example, Malinverni and others, 2014), but InSAR for snowy regions may be less negatively affected in areas where persistent scatterers (such as buildings) exist. One way to measure stability of a ground scatterer is a property called coherence that varies between 0 and 1, with 0 meaning that pixels in an image pair have no similarity and 1 indicating the pixels having high consistency over time. The coherence of SAR images is measured by the magnitude of cross-correlation of two SAR images (for example, Rosen and others, 2000). Figures 5 and 6 illustrate the coherence for selected date pairs in winter and summer. Coherence generally decreases as the time separation between images increases, the pixel size increases, and the radar wavelength decreases, among other variables (Rosen and others, 2000). It can be seen that coherence over the ESH site (small blue box) at this scale is fairly low during most periods, with slightly higher coherence for shorter-timescale interferograms (11- and 12- day pairs) than for the longer ones.

Snow cover and active rainfall (rain occurring at the time of the image acquisition) can both negatively impact InSAR time series, as they introduce both noise and potential biases to the individual interferograms. However, the lack of vegetation in winter can result in higher-quality interferograms spanning those time periods. Coherence in the winter 11 or 12 day pairs can be higher than in the summer because of the vegetation difference if there is not a change in the snow between the SAR acquisitions (Figures 5 and 6). We examined the impact of exclusion of snow covered images , as an effort to assess whether wintertime imagery improved or decreased the quality of the resulting inferred average deformation rates. We applied the StamPS method on two datasets. One dataset includes all the available images, and the other dataset includes only snow-/rain-free images. The snow covered images were determined using the Daily U.S. Snowfall and Snow Depth data provided by the National Centers for Environmental Information (www.ncdc.noaa.gov). There were a total of 25 snow-covered TSX images out of the original dataset of 80 scenes. Also, TSX images with precipitation (rain) more than 0.5 inches (3 images in total) were excluded from the dataset leaving 52 TSX images in our dataset of snow- and rain-free images. For S1 there were originally 49 scenes, with 31 in the snow and rain free dataset. The results showed that the snow-/rain-free data set results in a larger number of points inferred to be “stable” by the StaMPS approach– roughly twice the number of PS points as we find when all images are used. However, the average deformation rates inferred from the smaller snow-/rain-free dataset show a larger amount of scatter, potentially because the summer images tend to also have a larger contribution from tropospheric variability. Figures 7a and 7b illustrate our comparison between TSX and S1 results at the test site in Lansing. It is shown that S1-detected deformation rates are correlated with TSX-detected

deformation rates, with the same regions exhibiting high and low rates of deformation in both datasets. The correlation coefficients between the TSX and S1 data are similar to those found in a recent study in China (Wang and others, 2022). Figure 7 also illustrates high correlation (0.82 and 0.95, respectively, for S1 and TSX) between the deformation inferred from the full stack and snow-free datasets, suggesting that exclusion of the datasets impacted by snow and rain does not appear to result in a bias in the magnitude of the inferred average deformation rate.

Besides snow, interferogram quality can be degraded by the effect of changing vegetation cover. The persistent scatterers technique used by StaMPS should, theoretically, result in the selection of points where the contribution from vegetation is minimized. The ability of StaMPS and similar approaches to produce good estimates of pixel quality generally improves with larger numbers of images, although areas where the land use changes over time will continue to be challenging.

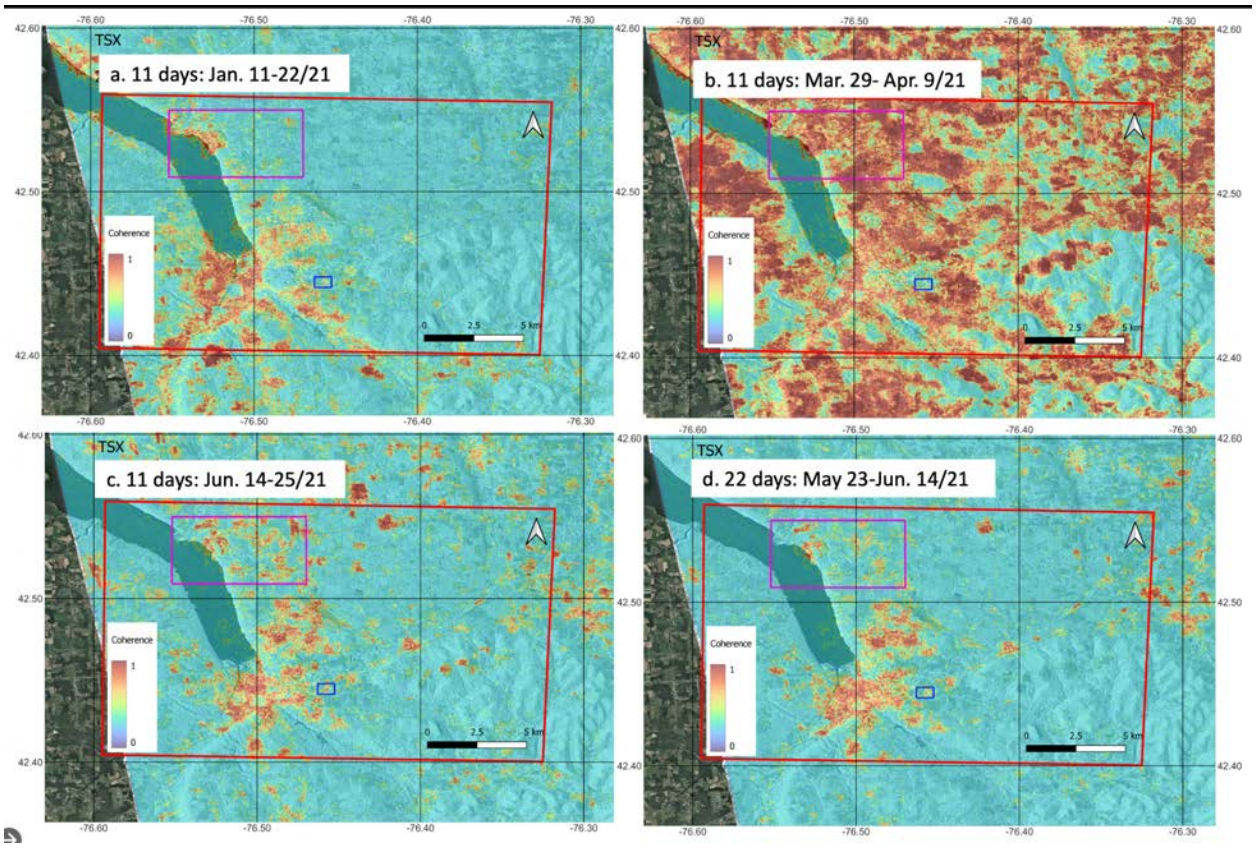

Figure 5. Coherence images of selected individual TSX interferograms showing radar signal similarity between image pairs in different seasons and over different periods of time (high similarity is red and close to 1): (a) 11 day winter pair; (b) 11 day early spring pair; (c) and (d) late spring pairs spanning 11 and 22 days. The SAR backscatter image is in the background. The purple square outlines the region shown in Figure 4 and the blue box is the region shown in Figure 12.

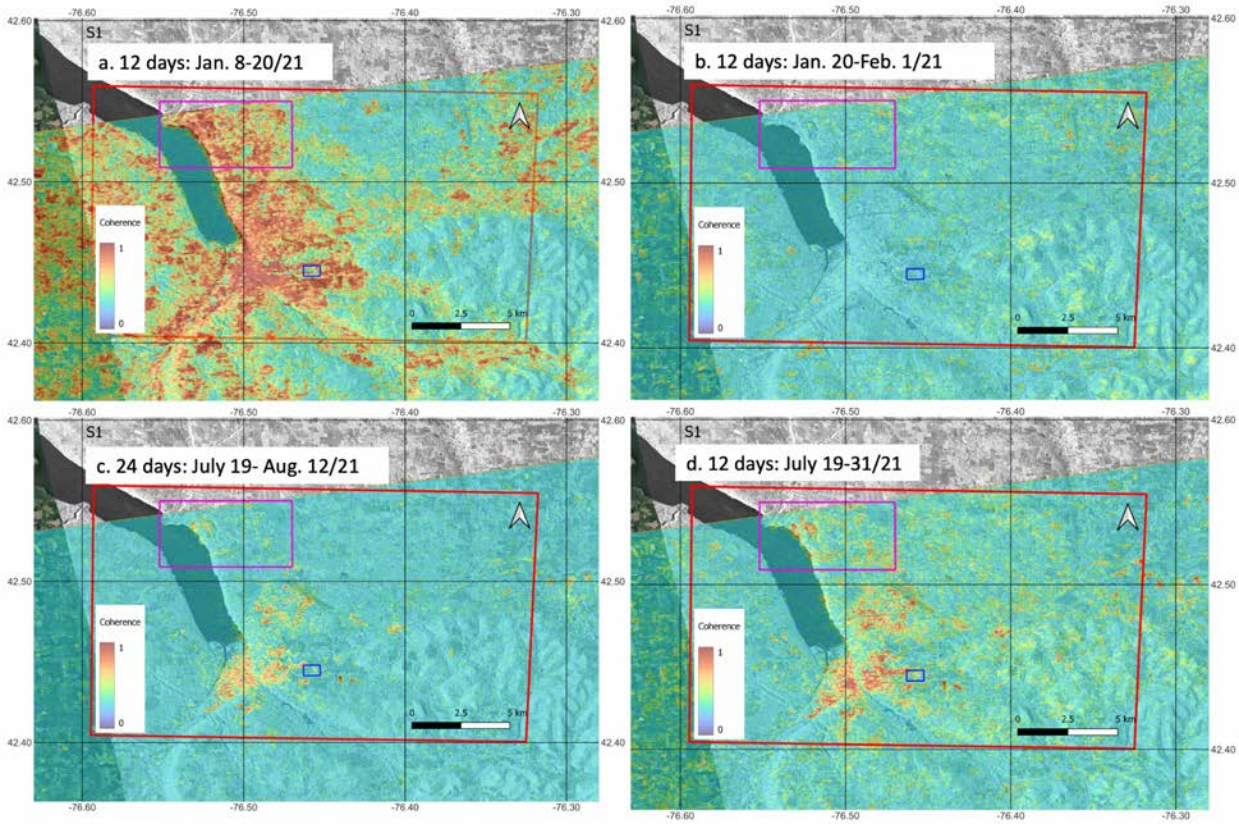

Figure 6. Coherence images of selected S1 interferograms showing radar signal similarity in different seasons and over different periods of time (high similarity is red and close to 1): (a) and (b) are different 12 day winter pairs with different coherence; (c) and (d) are summer pairs with 24 and 12 day separation. The SAR backscatter image is in the background. The purple square outlines the region shown in Figure 4 and the blue box is the region shown in Figure 12.

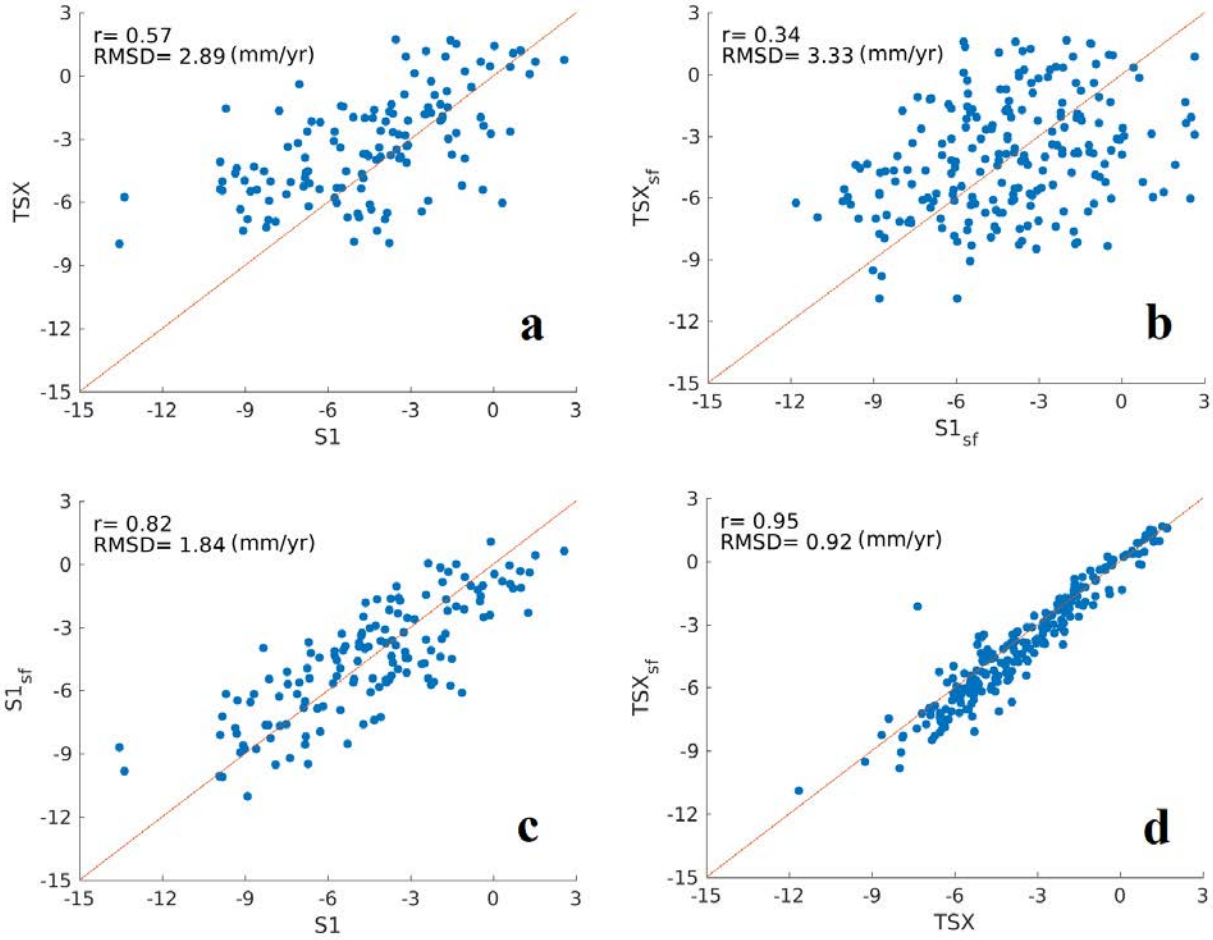

Figure 7. Scatter plot comparing displacement rates from the different satellites at the same measurement points for the Lansing test area shown in Figure 4 of a) TSX deformation versus S1 deformation, b) snow-/rain-free TSX deformation versus snow-/rain-free S1 deformation, c) S1 deformation versus snow-/rain-free S1 deformation, and d) TSX deformation versus snow-/rain-free TSX deformation. All the deformations are converted to vertical displacements assuming all motion is vertical using the incident angle of the radar beam. The numbers are in mm/yr and calculated for the timespan between January 2020 and August 2021. The root mean square difference (RMSD) between the datasets and the correlation coefficient between the datasets (r value) are shown. The red line shows the theoretical 1:1 line if the datasets were in perfect agreement.

4.2. Validation of InSAR results

Ground observations of elevation change data in our study area are shown in Figures 8-11, Table 1, and supplementary material. Multiple surveys were taken between 1979 and 2021 (Neves, 2015; Mark Rowe, personal communication, 2021), but in Figure 8 we present the time period with the best spatial coverage of the elevation change between 2014-2021 to overlap with the PSInSAR results. Because the satellite imagery spans a shorter time interval, 2018-2021, if the deformation rate has changed with time, we do not expect perfect agreement between the datasets. Further, as mentioned in section 3, the PSInSAR is sensitive to both horizontal and vertical components deformation while the ground control points can in theory, measure both separately (to different levels of accuracy). However, the longitude

and latitude of the surveyed points in 2014 and 2021 are the same, indicating that the horizontal was assumed fixed or no horizontal displacement was measured. Thus to compare the PSInSAR results with the ground-based observations, we have had to make the assumption that all deformation measured in the radar line of sight is vertical (see section 3).

Figures 9 and 10 show the comparison between ground measurements and PSInSAR observations. Figure 9 shows the comparison between the average rate inferred from the ground control points and PSInSAR measurements over time for eight selected points (see location of these points in Figure 8). Figure 10 illustrates the comparison between the average displacement rates inferred from the PSInSAR data with those of ground truth data for all points shown in Figure 11 as well as the subset of points in the area of highest deformation shown in Figure 8. TSX has closer agreement with the ground truth data (root mean squared difference of about 1.44 mm/yr) compared to S1 results (root mean squared difference of 1.92 mm/yr). However, considering all Ground Control Points (GCPs), the root mean squared differences for TSX and S-1 were 5.95 m/yr and 3.07 mm/yr, respectively. Agreement between concurrent GNSS and S1 results in China also finds root mean squared differences of 2-3 mm/yr (Wang and others, 2022).

To make the comparison between the PSInSAR and ground control points, we have to assume the datum used in the 2014 survey. While we have information about the techniques and vertical datum used in the 2021 survey, we do not have this information for the 2014 survey – we just have the benchmark number, latitude, longitude, and elevation. It is uncertain if the elevations in the 2014 survey were made with respect to NGVD29 (created in 1929) or NAVD88 (an update of the 1929 datum, created in 1988). We calculate two different sets of 2014-2021 displacement rates assuming the elevations in 2014 were with respect to the NGVD29 (Figure 11) and NAVD88 datums (not shown). The 2021 elevations in each datum were provided by Mark Rowe (personal communication, 2022). We find that the displacement rates from 2014-2021 assuming the NGVD29 datum for 2014 provide a better match to the PSInSAR results as well as the survey results from 1994-2014 (not shown). Based on this, we suspect that the 2014 survey elevations were made with respect to the NGVD29 datum. However, assuming the NGVD29 datum for the 2014 observations results in the displacements between 2014-2021 at seven points to be positive (uplift) – see point #75 in Table 1 and Figure 9 as well as all seven points in Figure 11. This uplift is surprising, because subsidence above the mined region is predicted for 200 years or more (Van Sambeek, 2013). The uplift is also observed at some of the same sites between 2004-2007 (Figure 11). While beyond the scope of this work, we think the uplift is not a true reflection of ground motion. Between 2004-2007 the uplift could be related to the benchmark K163 (used as a reference in all surveys, see Figure 1) being reset in 2006 according to the National Geodetic Survey data sheet (https://geodesy.noaa.gov/datasheets/). But we do not understand the cause of the apparent uplift between 2014-2021. One possible factor we are exploring in future work is the impact of seasonal ground deformation. The seasonal deformation can be possibly associated with elastic response to the loading effect of seasonal water level change of Cayuga lake and/or poroelastic response to groundwater fluctuations. We know the measurements in 2021 were taken in October, but are not sure about the measurements in 2014 (they are listed as being made on December 31, 1994, but this seems unlikely because of possible snow cover). If the 2014 measurements were made in a different season then it could have an impact of up to 10 mm on the elevation.

It should be noted that consistently higher subsidence rates between 1979 and 1994 compared to later measurements in 2004, 2007, 2014 might indicate a decline in mine closure rate with time, as expected from theoretical predictions (Van Sambeek, 2013). It should also be noted that, since InSAR observations

only can constrain displacement relative to other areas within the image (i.e., it is not an "absolute" measurement or displacement), we need to define a point or region as "zero" in each interferogram. Here we used the average value over a large area where we expect negligible deformation as the reference area. The reference area is marked "c" on the map in Figure 1. Any actual changes due to deformation with the reference region, as well as noise from the atmosphere or other sources, can introduce biases and noise to the resulting time series. We examined the results after using reference regions in other locations and found that there were no significant differences with the results shown here.

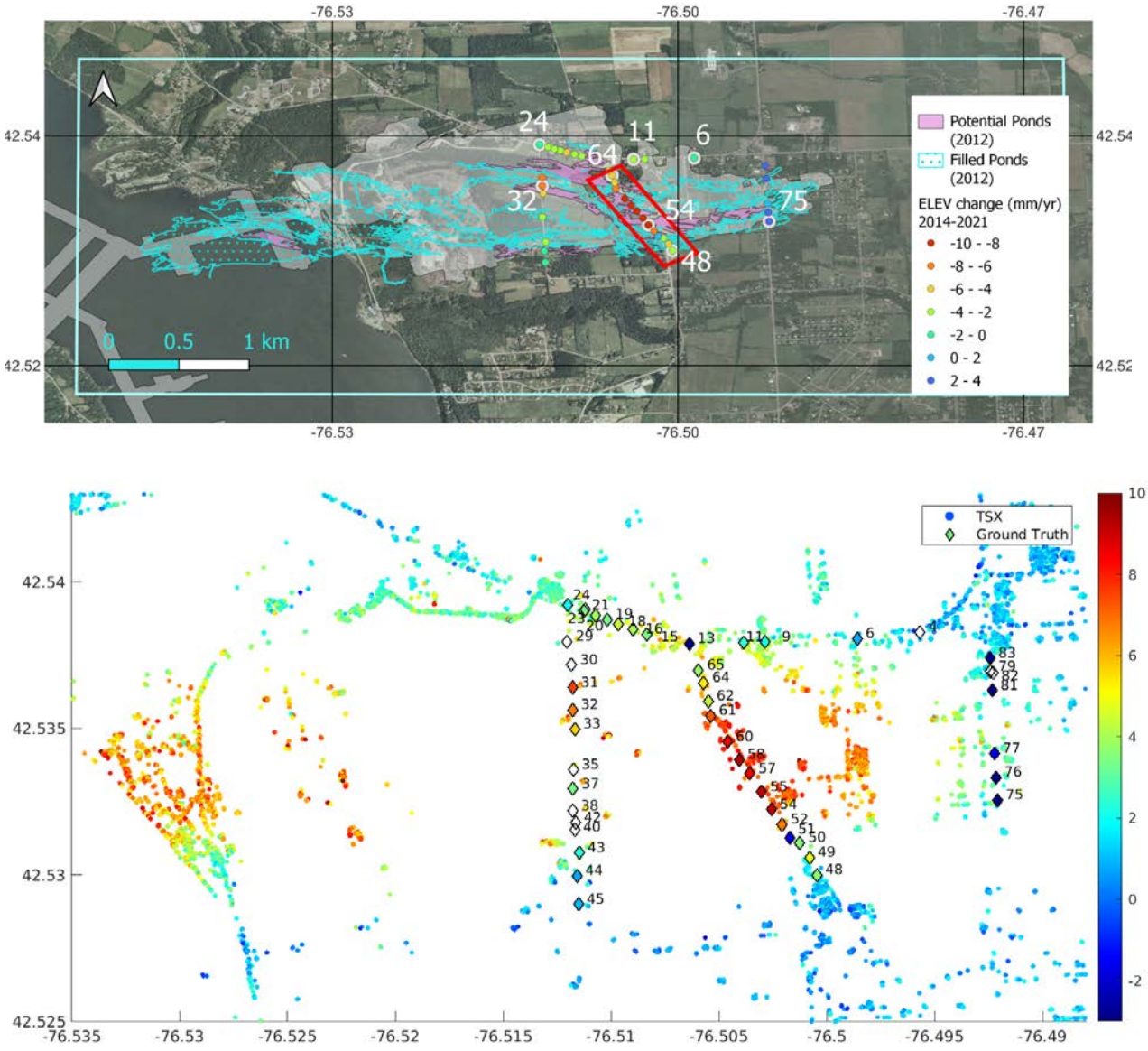

Figure 8. The elevation change in the Cayuga Salt Mine area. Top: Vertical elevation change between 2014-2021 measured by ground surveys (colored circles) overlaid on the extent of the mining area and individual salt tunnels (called salt ponds) (Cargill Deicing Technology, 2012). The area for the plots comparing the PSInSAR and ground survey results in Figure 10 is boxed in red. Eight numbered points selected for time series comparison in Figure 9 have white outlines. The ground measurements were conducted on Dec 31, 2014 by Spectra Surveying (Neves, 2015) and on Oct 13, 2012 by Keystone Associate, Binghamton. Bottom:

TSX PSInSAR inferred vertical ground velocity from 2018-2021 (colored dots) compared with all ground surveyed vertical velocities between 2014-2021 (colored diamonds labeled by GCP identification number).

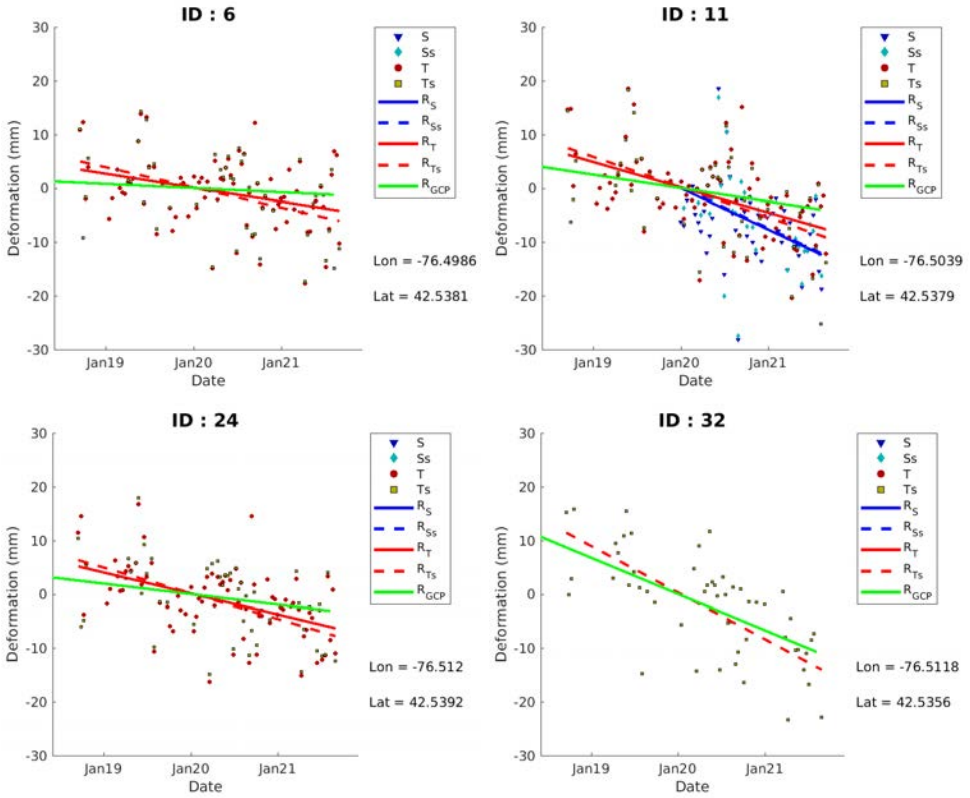

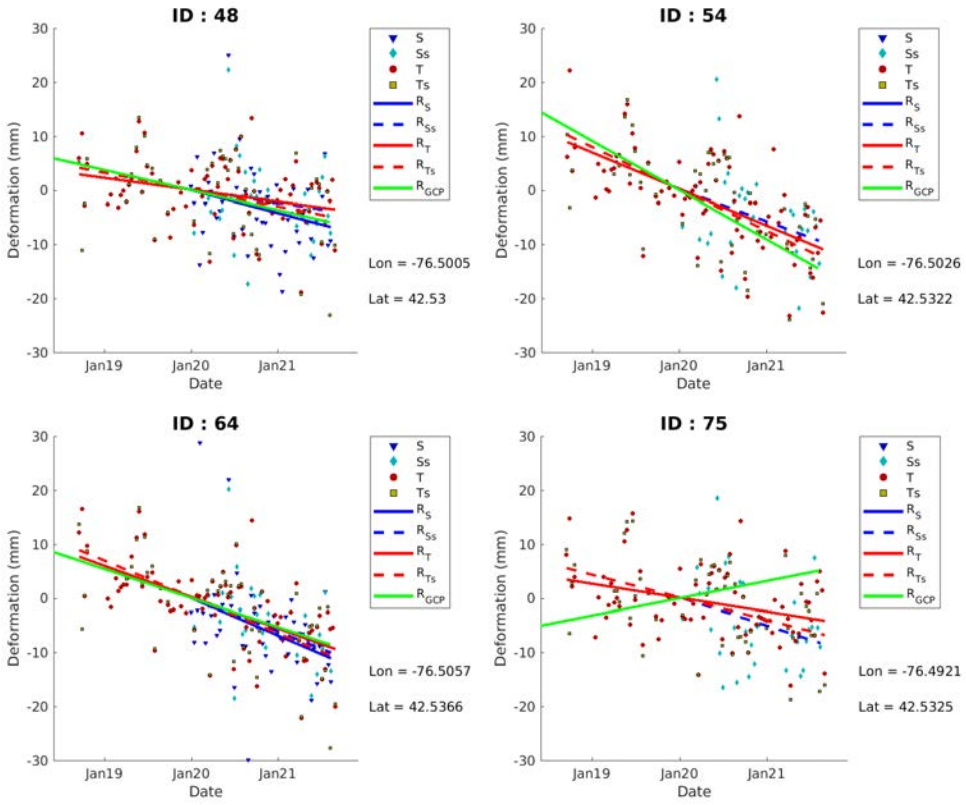

Figure 9. Time series of inferred vertical deformation at selected ground control points (see map in Figure 8) measured by different techniques. PSInSAR inferred elevations are shown as dots for S, S_s (spanning 2020-2021) and T, T_s, (for 2018-2021). Not every ground control point has all of the PSInSAR elevations within 25 m (for example, point 32 only has T_s). Linear fits to these points are R_{Ss}, R_T, R_{Ts}, R_{GCP}, respectively, the deformation rate for S, S_s, T, T_s, and GCP (the latter spanning 2014-2021). See Table 1 for the numeric values of these rates with error bounds.

Table 1. Deformation rate (mm/year) for the selected points in Figure 9. The error bounds (mm/year) are in parentheses.

	ID: 6	ID: 11	ID: 24	ID: 32	ID: 48	ID: 54	ID: 64	ID: 75
S1	-	-7.84 (1.54)	-	-	-4.30 (1.54)	-	-7.03 (1.54)	-
S1_srf	-	-7.67 (2.14)	-	-	-2.41 (2.14)	-5.90 (2.14)	-6.35 (2.14)	-5.25 (2.14)
TSX	-2.57 (0.54)	-4.68 (0.54)	-3.88 (0.54)	-	-2.18 (0.54)	-6.70 (0.54)	-5.77 (0.54)	-2.56 (0.54)
TSX_srf	-3.73 (0.65)	-5.60 (0.65)	-4.76 (0.65)	-8.61 (0.65)	-3.10 (0.65)	-7.68 (0.65)	-6.70 (0.65)	-4.17 (0.65)
GCP	-0.77 (5.06)	-2.47 (6.18)	-1.94 (7.91)	-6.70 (7.93)	-3.69 (6.06)	-9.03 (6.22)	-5.35 (6.61)	3.18 (4.12)

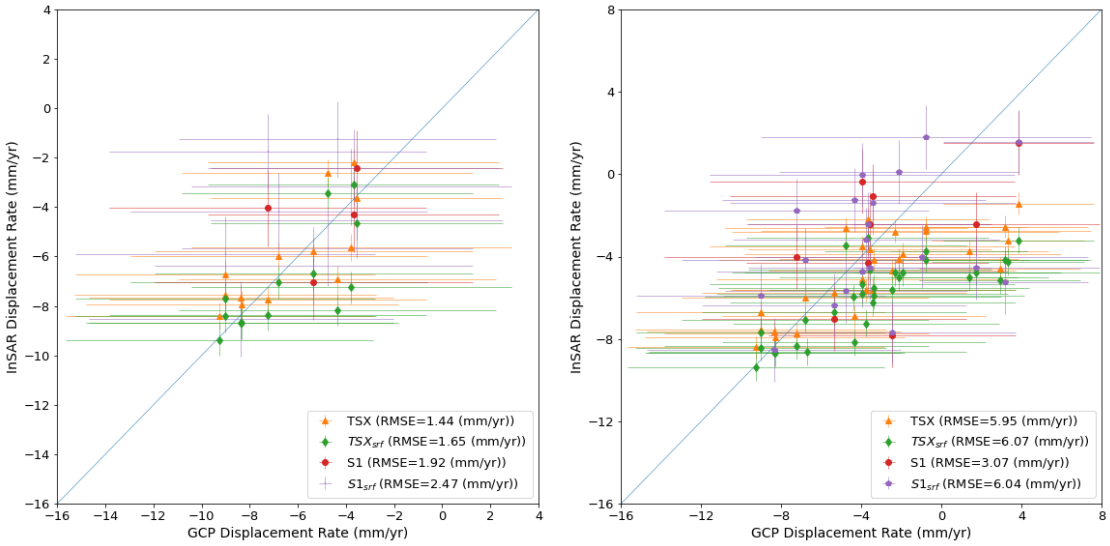

Figure 10. Scatterplot of TSX and Sentinel-1 deformation versus different subsets of the ground truth measurements made during an earlier time period, that is, elevation change between Dec 31, 2014, and Oct13, 2021. The location of the points are shown in figure 8. The root mean square difference (RMSD) between the PSInSAR and ground survey locations and the correlation coefficient between the datasets (r value) are shown. The blue line shows the theoretical 1:1 line if the datasets were in perfect agreement. See text for discussion of the error bounds. Left: Subset of 13 ground control points shown in red box in Fig. 8 in the most rapidly deforming area. Right: All GCPs (34) including uplifting points that we do not think are reliable (see text for discussion)

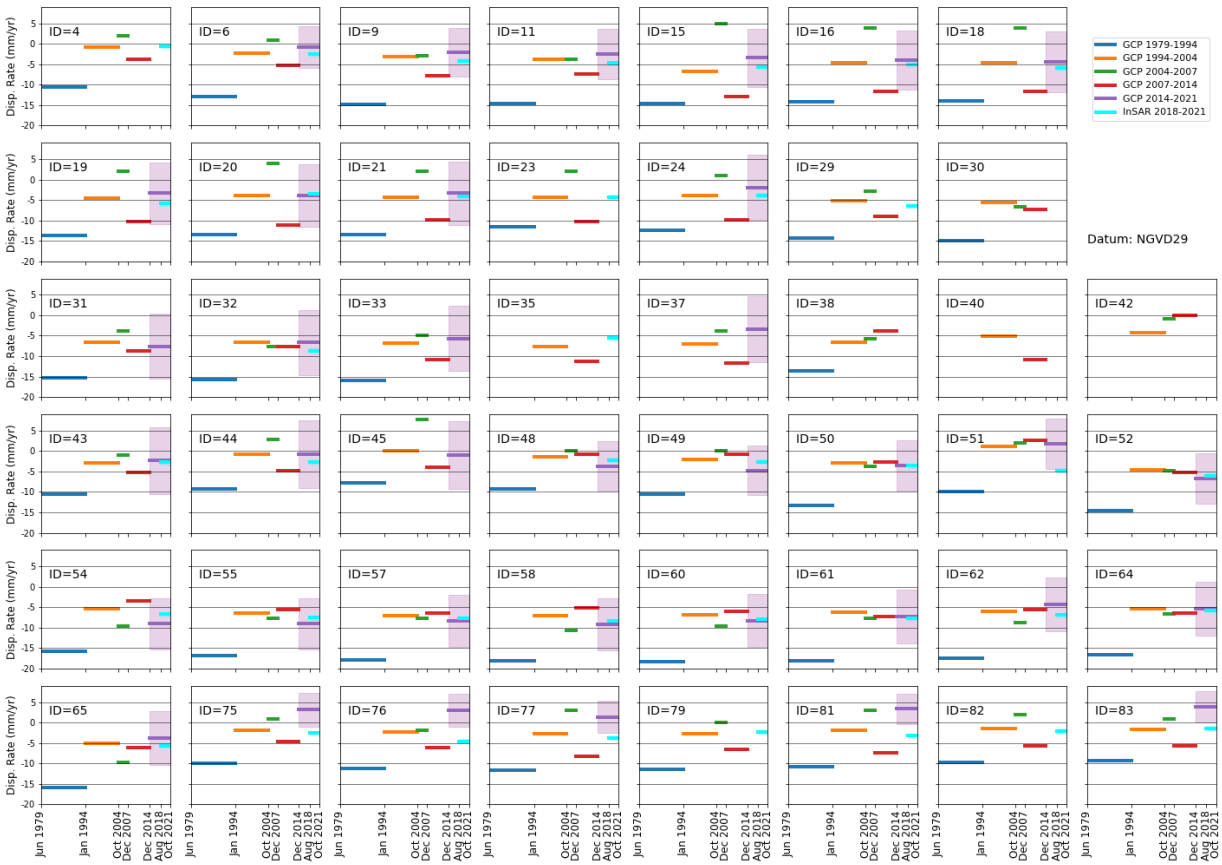

*Figure 11. Rates of ground motion over time from various ground surveys from 1979-2021 compared to PSInSAR (TerraSAR-X from 2018-2021) for 46 points assuming the NGVD29 datum for all ground surveys. Each point is labeled with the ID number (see Fig. 8 for map of locations). The uncertainty for each GCP measurement in 2021 is D*12.5 mm/km (Mark Rowe, personal communication, 2022), where D is its distance from the reference point of surveying, i.e., K163 (see Figure 1). We assume the errors are the same in 2014. The uncertainty of the GCP rate is calculated as* $\sqrt{2(D * 12.5)^2}$ *and is shown as a light purple region and calculated. Uncertainties for older GCP measurements are not known and so are not plotted. The uncertainty for PSInSAR measurement is calculated as RMSE of displacement rate over the area with assumed no/negligible deformation (see Figures 2, and 3), but are not visible when plotted at the scale of this plot.*

As another estimate of the precision of the results, we calculated the standard deviation of deformation rates in the area around the potential ESH drilling site (Figures 2 and 3) where we expect to observe negligible deformation at the current time. Any variability from zero that we do observe using current, pre-drilling data can be seen as a measure of the noise in the data as well as real variability (for example, seasonal signals) at the site. The standard deviations of the inferred displacement rates are 0.53, 0.55, 1.65, and 2.16 mm/year, respectively, for TSX, TSXsrf, S1, and S1srf. As we saw in the Lansing case, TSX has higher precision than the available S1 data. Also, the snow-/rain-free datasets possess lower precision values compared to the full-stack data. The difference is negligible, however, for TSX data. Based on this analysis, we estimate that TSX (with 36 months of data) can measure sub-mm/yr deformation rates while the S1 data cannot (with 20 months of data) over the ESH study area and that year round measurements of TSX can be used. However, since fewer S1 scenes were used, future work will address if a longer S1 time series with more dates is able to resolve sub-mm/yr deformation rates.

Figure 12. PSInSAR points and inferred vertical deformation rates near the proposed ESH drilling site are extracted using TSX (a), TSX_srf (b), S1 (c), and S1_srf images. The area shown in this figure is labeled "b" in Figure 1.

4.3. Feasibility of deformation mapping at ESH Drilling site

Surface movements have been observed in areas of geothermal production related to fluid pumping, injection, and leakage (for example, Lubitz and others, 2013; Heimlich and others, 2015; Semple and others 2017). Monitoring of surface deformation by InSAR could help assess if there is leakage and characterize where fluids are moving in the subsurface. For example, geothermal areas with nearly equal volumes of injection and pumping can still experience ground deformation if the pumping and reinjection are happening at different depths or locations (for example, Sorey and others, 1995). Here we assess whether the PS density around the proposed ESH site (Figure 12) would be able to detect possible scenarios involving deformation associated with subsurface geothermal well leakage such as observed in Landau, Germany (Heimlich and others, 2015). A leakage at a depth of 450 m in Landau caused ground uplift with a maximum of 3.5 cm over an area of about 8 km^2. The magnitude and extent of any potential deformation at the ESH site would be a function of the depth and rate of leakage, in addition to the geological and structural properties of the ground layers (i.e., how porous the surrounding rock is and how quickly any leaking fluid could move away from the site). Leakage at shallow depths would result in deformation over a smaller spatial scale than leakage at larger depths, all other things being equal. However, quantitative estimation of the expected deformation as a function of flow

rate would require a model to be developed based on the fluid properties and the geological and structural characteristics of the drilling site.

The proposed Cornell's ESH site is located in a parking lot where no persistent scatterers were found using the existing set of data. It can be seen in Figure 12 that in the area extending to about 200 m around the drilling site, there are quite a few TSX PS points that may allow the detection of possible deformation if it occurs with a magnitude and spatial scale similar to what was observed in Landau. In addition, there will be new buildings and facilities associated with ESH at the site that may provide more PS points. S1 has fewer PS points, but deformation at the scale of Landau would probably still be detectable. It should be noted that the temporal behavior of phase and amplitude of backscattered signals are used to select PS points but not the absolute value of the amplitude. However, the dimensions of a scatterer should be large enough (*e.g.,* at least at the scale of radar wavelength) to achieve a signal that is distinguishable from the background noise.

In addition, artificial radar reflectors, *i.e.,* corner reflectors or transponders, can be placed around the well area to provide reliable PS points. InSAR studies using corner reflectors as strong PS points with accurate measurements have been documented in, *e.g.,* Garthwaite, 2017 and Jauvin et al., 2019. The number, size, and the location of the corner reflector and also the feasibility of implementing corner reflectors in the study area should be assessed in future work.

The ESH site does not appear to be currently deforming within the precision of the TSX or S1 data – that is, the observed average displacement rates in the region are almost all below 1 mm/yr.

5. Conclusions

We used TSX and S1 satellite data and exploited Persistent Scatterer InSAR (PSInSAR) analysis using the StaMPS software to map ground velocities in Tompkins County between 2018-2021. PSInSAR using current satellites that collect images approximately every 11 or 12 days can detect mm/yr-scale deformation in Tompkins County, NY, when a year or more of data are used. The assessment of strain transients, or divergences from that average trend, can also be performed, potentially on a year-round basis, at a lower level of precision. We showed an example where we mapped known ground surface deformation of up to 10 mm/yr in the Lansing area associated with an underground salt mine. To evaluate the accuracy of results, we compared the measured deformation from the different satellites to each other and with ground control points that were acquired at earlier time periods. The S1 and TSX rate measurements are consistent with each other (root mean square difference of 3 mm/yr. However, TSX provides better spatial sampling because there are more persistent scatterers identified from within the TSX imagery. The comparison with 15 ground control points support our conclusion that the TSX data are more accurate (root mean square difference 1.44 mm/yr) compared to the S1 data (root mean square difference 1.92 mm/yr). In addition, we calculated the standard deviation of InSAR deformation rates for all datasets in the area around the drilling site where no current deformation is expected. Our analysis of the InSAR data confirms that there is little to no deformation occurring at the site at the current time - the standard deviation of the TSX observations at the site is 0.6 mm/yr and 2 mm/yr for S1. The results also showed that removing TSX and S1 images on the days of snow and rain did increase the number of persistent scatterers, but did not improve (and sometimes decreased) the precision of the deformation measurements.

Considering the results and the level of accuracy and precision observed within our test dataset, we suggest that the ESH project order TSX data with the maximum 11 day cadence for at least the 2-3 year period following the onset of injection activities at the site.

This study only used S1 data spanning from Jan 2020 to Aug 2021. An extended study using all possible data from S1 (which began acquiring data in late 2014) is suggested. Also, we suggest that other InSAR methods, for example multi-reference short baseline (SBAS) methods, are applied and the results be compared with the PSInSAR results in this study. Many of these approaches were developed for use on very different terrain and land use types, so it is not immediately obvious that one will perform better in Tompkins County than another. A strategy should be developed to exclude noisy dates from the time-series to improve our ability to estimate the deformation rate, as well as any excursions from it. The suggested studies should use the measured deformation over Cayuga Salt Mine to calibrate the method and evaluate the results.

Specific to the potential ESH geothermal project, a model should be developed based on the flow rate and the geological and structural properties of the study area to calculate the expected deformation as a function of leak depth and flow rate. We recommend further study to examine whether it is worth the cost to artificially improve the number of PS points around the well site. The number, size, and the location of corner reflectors or transponders and also the cost of implementing corner reflectors should be analyzed in the future work.

In addition, our results show deformation over several buildings in Tompkins County (visible in the supplemental csv files). Therefore, mapping and monitoring building subsidence can be a subject for an extended study.

Acknowledgements

We thank the Cornell Atkinson Center for Sustainability Academic Venture Fund for funding this work, the German Space Agency (DLR: Deutsches Zentrum für Luft- und Raumfahrt) for tasking and providing TerraSAR-X and TanDEM-X satellite data through project GEO3398, and the European Space Agency and Alaska Satellite Facility for providing the Sentinel-1 data. We thank John Dennis of the Cayuga Lake Environmental Action Network and Mark Rowe from Keystone Associates, Binghamton for sharing unpublished ground survey points from 2021. Older ground surveying data were obtained using a Freedom of Information Law request to the New York State Department of Environmental Conservation. We thank Jeff Tester, Teresa Jordan, Larry Cathles and Bert Bland for comments that improved the manuscript.

References

Bürgmann, R., Rosen, P. A., & Fielding, E. J. (2000). Synthetic aperture radar interferometry to measure Earth's surface topography and its deformation. *Annual review of earth and planetary sciences*, *28*(1), 169-209.

Cargill Deicing Technology. (2012). Brine Pond map contained in *Cargill 2011 Annual Report to NYSDEC on Cayuga Salt Mine* as georeferenced to the Google Earth surface landscape by cartographer Karen Edelstein for Cayuga Lake Environmental Action Now (CLEAN).

Crosetto M, Monserrat O, Cuevas-González M and others (2015). Measuring thermal expansion using X-band persistent scatterer interferometry. ISPRS J Photogramm Remote Sens 100:84–91

Del Soldato, M.; Confuorto, P.; Bianchini, S.; Sbarra, P.; Casagli, N. Review of Works Combining GNSS and InSAR in Europe. Remote Sens. (2021). 13, 1684. https://doi.org/ 10.3390/rs13091684

Ferretti, A., Prati, C., and Rocca, F. (2001). Permanent scatterers in SAR interferometry. IEEE TGRS, , 39(1), 8-20

Ferretti, A. *and others* (2007). Submillimeter Accuracy of InSAR Time Series: Experimental Validation. *IEEE Transactions on Geoscience and Remote Sensing*, vol. 45, no. 5, pp. 1142-1153, May 2007, doi: 10.1109/TGRS.2007.894440.

Garthwaite, M.C. On the Design of Radar Corner Reflectors for Deformation Monitoring in Multi-Frequency InSAR. Remote Sens. 2017, 9, 648.

Heimlich, C., Gourmelen, N., Masson, F., Schmittbuhl, J., Kim, S. W., and Azzola, J. (2015). Uplift around the geothermal power plant of Landau (Germany) as observed by InSAR monitoring. *Geothermal Energy, 3(1), 2.*

Hooper, A., Segall, P., and Zebker, H. (2007). Persistent Scatterer InSAR for Crustal Deformation Analysis, with Application to Volcan´ Alcedo, Galapagos. *Journal of Geophysical Research, Solid Earth.*

Jauvin, M.; Yan, Y.; Trouvé, E.; Fruneau, B.; Gay, M.; Girard, B. Integration of Corner Reflectors for the Monitoring of Mountain Glacier Areas with Sentinel-1 Time Series. Remote Sens. 2019, 11, 988.

Lubitz, C., Motagh, M., Wetzel, H. U., and Kaufmann, H. (2013). Remarkable urban uplift in Staufen im Breisgau, Germany: Observation from TerraSAR-X InSAR and leveling from 2008 to 2011. *Remote Sensing*, 5(6), 3082-3100.

Malinverni, E. S., Sandwell, D. T., Tassetti, A. N., & Cappelletti, L. (2014). InSAR decorrelation to assess and prevent volcanic risk. *European Journal of Remote Sensing*, *47*(1), 537-556.

McClusky, S., & Tregoning, P. (2013). Background paper on subsidence monitoring and measurement with a focus on coal seam gas (CSG) activities. Report to New South Wales Chief Scientist and Engineer. Canberra, Australia. 43 pp.
https://www.chiefscientist.nsw.gov.au/__data/assets/pdf_file/0016/33028/Subsidence-Monitoring_McClusky-Tregoning_ANU.pdf

Neves, Mark. (2015). Subsidence worksheet for Cayuga Salt Mine. Survey conducted by Spectra Environmental Group, Inc. on Dec 31, 2014, as released to John V. Dennis in response to FOIL request to NYSDEC No. W033975-032218. 6 pp.
Rosen, P. A., Hensley, S., Joughin, I. R., Li, F. K., Madsen, S. N., Rodriguez, E., & Goldstein, R. M. (2000). Synthetic aperture radar interferometry. *Proceedings of the IEEE*, *88*(3), 333-382.

Rosen, P. A., Gurrola, E., Sacco, G. F., & Zebker, H. (2012). The InSAR scientific computing environment. In *EUSAR 2012; 9th European Conference on Synthetic Aperture Radar* (pp. 730-733). VDE.

Sandwell, D.T.; Myer, D.; Mellors, R.; Shimada, M.; Brooks, B. Foster, J. (2008). Accuracy and Resolution of ALOS Interferometry: Vector Deformation Maps of the Father's Day Intrusion at Kilauea. IEEE Trans. Geosci. Remote Sens. 46, 3524–3534.

Semple, A. G., Pritchard, M. E., & Lohman, R. B. (2017). An incomplete inventory of suspected human-induced surface deformation in North America detected by satellite interferometric synthetic-aperture radar. Remote Sensing, 9(12). https://doi.org/10.3390/rs9121296

Sorey, M. L., Farrar, C. D., Marshall, G. A., & Howie, J. F. (1995). Effects of geothermal development on deformation in the Long Valley Caldera, eastern California, 1985–1994. Journal of Geophysical Research: Solid Earth, 100(B7), 12475-12486.

Spectra Environmental Group, Inc. in collaboration with Sear-Brown and RESPEC (2000) CARGILL CAYUGA MINE EXPANDED ENVIRONMENTAL ASSESSMENT Volume II, Latham, New York.

Valentino, B. (2016) Application of InSAR to salt mine subsidence, M.S. thesis, Cornell University, 98 pp. https://ecommons.cornell.edu/bitstream/handle/1813/45136/brv9.pdf?sequence=1

Van Sambeek, L. L. (2013) Expected Subsidence Over the Cayuga Mine Amended Area, Topical Report RSI-2361, RESPEC, Rapid City South Dakota

Wang, Y., Feng, G., Li, Z., Xu, W., Zhu, J., He, L., Xiong, Z. and Qiao, X. (2022). Retrieving the displacements of the Hutubi (China) underground gas storage during 2003–2020 from multi-track InSAR. *Remote Sensing of Environment*, *268*, p.112768.

Supplemental Material

We include csv files of the ground displacements in the radar line of sight along with the appropriate latitude and longitude for both the TSX (30 files combined in a zip file) and S1 datasets (1 file: Patch 12). Because of the size of the files, this has been broken into a series of patches for each dataset and a reference map showing the location of each patch is provided as Supplemental Figures 1 and 2.

Supplemental Figures 3-36 show the time series of the PSInSAR points that are within 25 m of a ground survey point (surveyed in 2014 and 2021) for 33 of the points where such comparisons can be made. Each plot is labeled by the id # of the ground surveyed point. The right side of each figure shows the same map as Fig. 8, but the location of the time series shown on the left side is labeled with a pink star. On the left, we include the TerraSAR-X time series (labeled T, used in Fig. 2) along with other time series available at this point. The points labeled Ts are from the TerraSAR-X time series only including satellite data overpasses from snow or rain free days. The points labeled S or Ss are from the Sentinel-1 satellite during all dates or rain/snow free dates, respectively. Our analysis is that the rates from the rain/snow free dates are not significantly different from the rates calculated using all the dates. However, the advantage of the rain/snow free analysis is that it allows measurements at a few points where results are not possible with the full dataset -- for example ground ID #18 only has the TerraSAR-X snow/rain

free time series, but no Sentinel-1 PSInSAR data were available for this point. The lines labeled "R" are the rates calculated from the data points. GCP = Ground control points surveyed in 2014-2021.

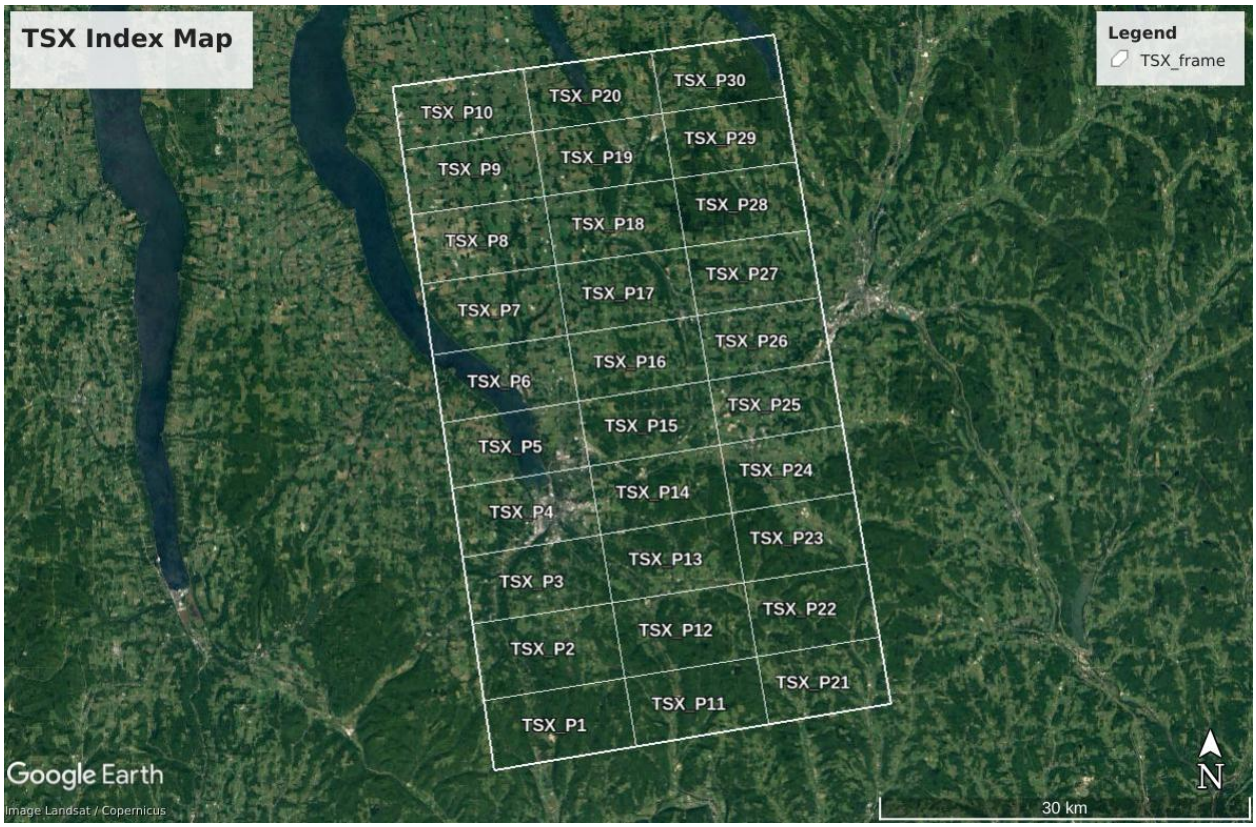

Supplemental Figure 1. Locations of the patches of the processed TSX displacement rates at the persistent scatterer points as 30 csv files.

Supplemental Figure 2. Location of the patch 12 of the processed Sentinel-1 displacement rates at the persistent scatterer points as a Sentinel-1 csv file.